

# Microstructural Characterization of Polystyrene-*block*-poly(ethylene oxide)-Templated Silica Films with Cubic-Ordered Spherical Mesopores

Bernd Smarsly,<sup>†,‡</sup> George Xomeritakis,<sup>\*,†</sup> Kui Yu,<sup>\*,§</sup> Nanguo Liu,<sup>†</sup> Hongyou Fan,<sup>§</sup> Roger A. Assink,<sup>§</sup> Celeste A. Drewien,<sup>§</sup> Wilhelm Ruland,<sup>||</sup> and C. Jeffrey Brinker<sup>†,§</sup>

Center for Microengineered Materials, Advanced Materials Laboratory, University of New Mexico, 1001 University Boulevard SE, Suite 100, Albuquerque, New Mexico 87106, Sandia National Laboratories, MS 1349, Albuquerque, New Mexico 87185, and Department of Chemistry and Centre of Materials Sciences, University of Marburg, D-35032 Marburg, Germany

Received May 9, 2003. In Final Form: June 13, 2003

We report the synthesis and characterization of mesostructured thin silica films derived from methyltriethoxysilane (MTES) and/or tetraethyl orthosilicate (TEOS) silica precursors and polystyrene-*block*-poly(ethylene oxide) (PS-*b*-PEO) diblock copolymers via the solvent evaporation-induced self-assembly (EISA) process. It is found that the meso- and microstructure of the calcined films consists of cubic-ordered arrays of spherical mesopores of 5–7 nm in diameter, interconnected with a small number ( $\leq 4\%$  by volume) of PEO-induced micropores of  $\sim 1$  nm in diameter, as determined by new experimental results of transmission electron microscopy,  $N_2$  sorption, gas permeation, and grazing incidence small-angle X-ray scattering studies. The present comprehensive study of these novel closed-pore films should provide a general methodology for microstructural characterization of other related porous films prepared by similar self-assembly processes.

## 1. Introduction

Since their discovery by Mobil researchers in 1992,<sup>1</sup> mesoporous inorganic oxides prepared by supramolecular self-assembly have attracted a great interest both from a fundamental point of view as well as for potential applications as catalysts, sorbents, or low  $k$  dielectrics.<sup>2,3</sup> The preparation of such materials in the form of thin films has been studied extensively, in particular by Brinker and co-workers<sup>4</sup> and Grosso and co-workers,<sup>5</sup> by means of

low-molecular weight surfactants as structure-directing agents through solvent evaporation-induced self-assembly (EISA).

Recently, we reported on the preparation of mesostructured silica thin films with a large characteristic length scale by using a high molecular weight amphiphilic block copolymer, e.g., polystyrene-*block*-poly(ethylene oxide) (PS-*b*-PEO), as structure-directing agent.<sup>6</sup> It was shown that various mesostructures could be obtained including regular and inverted ones. The reported system is believed to be the first to use high glass transition temperature ( $T_g \approx 373$  K), PS-based amphiphilic diblock copolymers to prepare mesostructured silica/amphiphile films with highly ordered mesophases through the EISA process.

In our most recent publication,<sup>6b</sup> we reported on the self-assembly and mesostructural characterization of hydrophobic silica films with cubic-ordered spherical mesopores, using the same PS-*b*-PEO copolymer as structure-directing agent and methyltriethoxysilane (MTES) as silica source. While this study elucidated the pore size, shape, and 3D arrangement of the mesopores, it provided only limited information about the microstructure, porosity, and pore connectivity of the silica matrix surrounding the mesopores. Previous studies showed that siliceous materials in general could contain

\* Corresponding authors. G.X.: fax (505) 272-7336; e-mail xomerita@unm.edu. K.Y.: Present address Steacie Institute for Molecular Sciences, National Research Council, 100 Sussex Drive, Ottawa, Ontario Canada K1A 0R6; e-mail kui.yu@nrc.ca.

<sup>†</sup> University of New Mexico.

<sup>‡</sup> Present address: Max Planck Institute of Colloids and Interfaces, Research Campus Golm, D-14424 Potsdam, Germany.

<sup>§</sup> Sandia National Laboratories.

<sup>||</sup> University of Marburg.

(1) Kresge, C.; Leonowicz, M.; Roth, W.; Vartuli, C.; Beck, J. *Nature* **1992**, *359*, 710.

(2) (a) Ogawa, M. *J. Am. Chem. Soc.* **1994**, *116*, 7941. (b) Huo, Q.; Margolese, D. I.; Clesla, U.; Feng, P.; Gler, T. E.; Slegler, P.; Leon, R.; Petroff, P. M.; Schuth, F.; Stucky, G. D. *Nature* **1994**, *368*, 317. (c) Tanev, P. T.; Pinnavaia, T. J. *Science* **1995**, *267*, 865. (d) Markus, T.; Franck, A.; Chesne, A. D.; Leist, H.; Zhang, Y.; Ulrich, R.; Schadler, V.; Wiesner, U. *Science* **1997**, *278*, 1795.

(3) (a) Antonelli, D. M.; Ying, J. Y. *Angew. Chem., Int. Ed. Engl.* **1995**, *34*, 2014. (b) Mann, S.; Ozin, G. A. *Nature* **1996**, *382*, 313. (c) Ozin, G. A.; Chomski, E.; Khushalani, D.; Maclachlan, M. J. *Curr. Opin. Colloid Interface Sci.* **1998**, *3*, 181. (d) Brinker, C. J.; Lu, Y.; Sellinger, A.; Fan, H. *Adv. Mater.* **1999**, *11*, 579. (e) Hillhouse, H. W.; van Egmond, J. W.; Tsapatsis, M. *Langmuir* **1999**, *15*, 4544. (f) Hillhouse, H. W.; van Egmond, J. W.; Tsapatsis, M. *Chem. Mater.* **2000**, *12*, 2888.

(4) (a) Lu, Y.; Ganguli, R.; Drewien, C.; Anderson, M.; Brinker, C.; Gong, W.; Guo, Y.; Soye, H.; Dunn, B.; Huang, M.; Zink, J. *Nature* **1997**, *389*, 364. (b) Sellinger, A.; Weiss, P. M.; Nguyen, A.; Lu, Y.; Assink, R. A.; Gong, W.; Brinker, C. J. *Nature* **1998**, *394*, 256. (c) Fan, H.; Lu, Y.; Stump, A.; Reed, S. T.; Baer, T.; Schunk, R.; Perez-Luna, V.; López, G. P.; Brinker, C. J. *Nature* **2000**, *405*, 56. (d) Doshi, D. A.; Huesing, N. K.; Lu, M.; Fan, H.; Lu, Y.; Simmons-Potter, K.; Potter, B. G.; Hurd, A. J.; Brinker, C. J. *Science* **2000**, *290*, 107.

(5) (a) Grosso, D.; Balkenende, A. R.; Albouy, P. A.; Ayrál, A.; Amenitsch, H.; Babonneau, F. *Chem. Mater.* **2001**, *13*, 1848. (b) Cagnol, F.; Grosso, D.; Soler-Illia, G. J. D. A. S.; Crepaldi, E. L.; Babonneau, F.; Amenitsch, H.; Sanchez, C. *J. Mater. Chem.* **2003**, *13*, 61–66. (c) Grosso, D.; Babonneau, F.; Sanchez, C.; Soler-Illia, G. J. D. A.; Crepaldi, E. L.; Albouy, P. A.; Amenitsch, H.; Balkenende, A. R.; Brunet-Bruneau, A. *J. Sol-Gel Sci. Technol.* **2003**, *26*, 561. (d) Grosso, D.; Balkenende, A. R.; Albouy, P. A.; Ayrál, A.; Amenitsch, H.; Babonneau, F. *Chem. Mater.* **2001**, *13*, 1848.

(6) (a) Yu, K.; Hurd, A. J.; Eisenberg, A.; Brinker, C. J. *Langmuir* **2001**, *17*, 7961. (b) Yu, K.; Smarsly, B.; Brinker, C. J. *Adv. Funct. Mater.* **2003**, *13* (1), 47–52.

solvent-induced micropores of  $\sim 0.3\text{--}0.4$  nm in size.<sup>7</sup> In addition, templated silicas prepared with PS-*b*-PEO as structure-directing agent can possess additional micro-porosity of  $\sim 1$  nm in diameter, originating from partial extension of the PEO chains inside the silica matrix.<sup>8,9</sup> The size, amount, and connectivity of these micropores with the diblock-templated mesopores could affect certain macroscopic properties of the films (moisture adsorption, dielectric constant, etc.) and is of fundamental interest regarding the role of such copolymers in pore formation during self-assembly.

In view of the above, the objective of the present study is to investigate in detail the following aspects of the meso- and microstructure of our diblock-templated films:

- (1) Do the mesopores form an interconnected network throughout the films?
- (2) Are there any micropores present in the silica matrix surrounding the mesopores?
- (3) What is the volume fraction of these micropores?
- (4) Are the mesopores interconnected through these micropores?

To provide answers to these fundamental questions regarding the pore structure and connectivity in films with ordered mesopores, we employed a number of independent characterization techniques including thin-film nitrogen sorption, grazing incidence small-angle X-ray scattering (GISAXS), and gas permeation. Thin-film nitrogen sorption is particularly useful to determine whether the templated mesopores of our films form an interconnected network throughout the film thickness. GISAXS measurements at large scattering angle of the diblock-templated silica films as well as reference films templated with PEO homopolymer can provide quantitative information regarding the presence of PEO-induced micropores in the silica matrix of the former. Finally, single-component permeation experiments of a series of gases of different kinetic diameter or gas permeation in the presence of condensable vapors can provide semi-quantitative information on the size (spanning the range of 0.3–10 nm) of accessible pores of templated films deposited on porous supports.

In what follows, a comprehensive characterization is presented of the meso- and microstructure of MTES- and/or TEOS-derived, diblock-templated silica films by TEM, nitrogen sorption, gas permeation and GISAXS experiments, thus suggesting a general methodology for characterization of other related thin-film materials with similarly intricate (meso- or micro-) pore structures.

## 2. Experimental Section

**2.1. Synthesis of Templated and Nontemplated Silica Films.** The preparation of the templated films was carried out as described in detail in ref 6, with pure MTES, a 40:60 (w/w) MTES/TEOS mixture, or pure TEOS as the silica precursor. Nontemplated silica films were prepared under similar conditions

but without adding the PS-*b*-PEO diblock copolymer. Also, microporous templated silica films were prepared using PEO homopolymer as pore template, with PEO/TEOS weight ratios of 1/11 or 1/3.

**2.2. TEM and N<sub>2</sub> Sorption.** The mesostructure of the as-cast and calcined silica films were directly observed on a Jeol 2010 transmission electron microscope (TEM) operated at an acceleration voltage of 200 kV. The samples for TEM were prepared by scratching the films with a pair of tweezers and directly dispersing the film fragments onto holey carbon-coated copper grids.

Thin-film N<sub>2</sub> sorption measurements at 77 K were performed with a homemade surface acoustic wave (SAW) device integrated into a commercial porosimeter (ASAP 2010, Micromeritics). Each film was applied on  $\sim 1$  cm<sup>2</sup> area of a piezoelectric quartz substrate with Ti-primed gold transducers designed to operate at  $\sim 97$  MHz. Mass change as a function of N<sub>2</sub> relative pressure was determined from the frequency shift of the SAW device (sensitivity  $\sim 80$  pg/cm<sup>2</sup>). More details for the characterization of porous films by the SAW technique are described in detail elsewhere.<sup>10</sup>

**2.3. Gas Permeation.** The gas transport properties of TEOS- or MTES-derived PS-*b*-PEO- and PEO-templated silica films deposited on commercial, porous 50 Å  $\gamma$ -Al<sub>2</sub>O<sub>3</sub> disk supports (Inocermic, Germany) were measured with a custom-made, stainless steel membrane holder with elastomer O-ring seals. The side of the support disk coated with the silica membrane was flushed with a gas stream of interest at a flow rate of 100 cm<sup>3</sup>/min and a pressure of 50–100 kPa above ambient. The amount of gas permeating through the membrane was detected from the opposite side at ambient pressure with the aid of a calibrated soap-film flowmeter. The probe gases of interest were He (2.6 Å), CO<sub>2</sub> (3.3 Å), N<sub>2</sub> (3.64 Å), CH<sub>4</sub> (3.8 Å), and SF<sub>6</sub> (5.5 Å), in order of increasing kinetic diameter. The membrane permeance for each gas was defined as the flow rate of permeating gas (cubic centimeters per minute) divided by the available area for permeation (square centimeters) and the pressure difference (atmospheres) from the feed to the permeate side of the membrane.

In addition to single-gas permeation experiments, we also contacted permeation studies in the presence of a condensable vapor, here ethanol, which is more suitable to semiquantify pore sizes in the range 1–10 nm. In this type of operation mode, which is often denoted as permoporosimetry,<sup>11</sup> the permeation rate of a nonadsorbing gas (N<sub>2</sub>, Ar) through the membrane is measured as a function of increasing relative pressure ( $P/P_{\text{sat}}$ ) of ethanol vapor introduced from both sides of the membrane. In this manner, when the relative pressure of ethanol matches the critical pressure to achieve pore condensation, a complete blockage of permeation of the nonadsorbing gas is achieved, which can be used to estimate the average pore size of the membrane.

**2.4. SAXS Investigation.** Both the meso- and microstructures of the thin-film samples were studied by small-angle X-ray scattering (SAXS) on the pinhole rotating-anode instrument (Rotaflex, Rigaku, 4 W, CuK $\alpha$ ) in our in-house SAXS facility. A special sample holder was constructed and utilized to study thin-film samples in grazing incidence geometry (GISAXS). In this way, it was possible to adjust the angle of incidence of the primary X-ray beam to approach the angle of total reflection of thin-film samples, thereby getting maximum scattering intensity. A 2D wire detector was used, and the sample was kept under vacuum during the measurement. The range of available values for the scattering vector  $s$  was  $s = 0.05\text{--}1.4$  nm<sup>-1</sup>, where  $s = 2 \sin(\theta)/\lambda$ ,  $2\theta$  is the scattering angle, and  $\lambda$  is the CuK $\alpha$  wavelength. A number of trial GISAXS experiments were also carried out in the synchrotron facility at Brookhaven National Laboratory, but that particular setup did not allow a sufficiently large sample-detector distance to get better 2D GISAXS patterns than those obtained with our in-house SAXS facility.

The analysis of the experimental GISAXS data acquired in this study should in general be performed with more caution, as compared to "classical" SAXS in transmission mode, mainly due

(7) (a) de Vos, R. M.; Verweij, H. *J. Membr. Sci.* **1998**, *143*, 37. (b) de Vos, R. M.; Maier, W. F.; Verweij, H. *J. Membr. Sci.* **1999**, *158*, 277. (c) Tsai, C. Y.; Tam, S. Y.; Lu, Y.; Brinker, C. J. *J. Membr. Sci.* **2000**, *169*, 255. (d) Xomeritakis, G.; Naik, S.; Braunbarth, C. M.; Cornelius, C. J.; Pardey, R.; Brinker, C. J. *J. Membr. Sci.* **2003**, *215*, 225.

(8) Paul, S. M. D.; Zwanziger, J. W.; Ulrich, R.; Wiesner, U.; Spiess, H. W. *J. Am. Chem. Soc.* **1999**, *121*, 5727.

(9) (a) Smarsly, B.; Goltner, C.; Antonietti, M.; Ruland, W.; Hoinakis, E. *J. Phys. Chem. B* **2001**, *105*, 831. (b) Smarsly, B.; Polarz, S.; Antonietti, M. *J. Phys. Chem. B* **2001**, *105*, 10473. (c) Goltner, C. G.; Smarsly, B.; Berton, B.; Antonietti, M. *Chem. Mater.* **2001**, *13*, 1617. (d) Tattershall, C. E.; Jerome, N. P.; Budd, P. M. *J. Mater. Chem.* **2001**, *11*, 2979–2984. (e) Tattershall, C. E.; Aslam, S. J.; Budd, P. M. *J. Mater. Chem.* **2002**, *12*, 2286–2291. (f) Joo, S. H.; Ryoo, R.; Kruk, M.; Jaroniec, M. *J. Phys. Chem. B* **2002**, *106*, 4640–4646. (g) Ryoo, R.; Ko, C. H.; Kruk, M.; Antochshuk, V.; Jaroniec, M. *J. Phys. Chem. B* **2000**, *104*, 11465–11471.

(10) Frye, G. C.; Ricco, A. J.; Martin, S. J.; Brinker, C. J. *Mater. Res. Soc. Symp. Proc.* **1988**, *121*, 349.

(11) (a) Tsuru, T.; Hino, T.; Yoshioka, T.; Asaeda, M. *J. Membr. Sci.* **2001**, *186*, 257. (b) Tsuru, T.; Takata, Y.; Kondo, H.; Hirano, F.; Yoshioka, T.; Asaeda, M. *Separ. Purif. Technol.* **2003**, *32*, 23.

to the very low angles of incidence of the primary beam employed in this operation mode. For example, for angles of incidence lower than the critical angle,  $\theta_{cr}$ , the primary beam undergoes total reflection, while for  $\theta > \theta_{cr}$  the beam enters the sample resulting in scattering contribution proportional to  $1/\theta^4$ , superimposed with the scattering from the film meso- or microstructure. However, for the particular samples considered here these contributions are negligible compared to the scattering from the high internal surface area of the film meso- or micropores, as verified with the well-characterized porous silica powder described in ref 9. More details and considerations on GISAXS data analysis and interpretation of oriented mesoporous structures are given in detail elsewhere.<sup>12</sup>

### 3. SAXS Simulation

To elucidate the influence of the MTES methyl ligands and PEO micropores on the GISAXS patterns of MTES- and MTES/TEOS-derived nontemplated silica films, SAXS simulations were developed with suitable assumptions for the distribution of the methyl ligands and micropores. In principle, SAXS data of the MTES-derived, PS-*b*-PEO templated mesoporous silica films have to be interpreted in terms of a three-phase system with respect to domains of different average electron density. The three different components are the pores (mesopores and micropores), the CH<sub>3</sub>- units, and the SiO<sub>2</sub> matrix. It is assumed that the shape of the SAXS curve at large  $s$  is not significantly influenced by the interparticulate scattering from the mesopores. Assuming that no spatial correlation exists between the CH<sub>3</sub> units, the mesopores, and any micropores, the theoretical SAXS of the matrix, containing micropores and CH<sub>3</sub> groups, at large  $s$  is approximated by

$$I(s) = \rho'_{\text{micro}}{}^2 \phi_{\text{micro}} I_{\text{micro}}(s) + \rho'_{\text{methyl}}{}^2 \phi_{\text{methyl}} I_{\text{methyl}}(s) \quad (1)$$

where  $\phi_i$  and  $I_i(s)$  are the volume fractions and theoretical SAXS intensity of the methyl groups and the PEO micropores. The relative electron densities are defined by  $\rho'_{\text{micro}} = \rho_{\text{micro}} - \rho_0$  and  $\rho'_{\text{methyl}} = \rho_{\text{methyl}} - \rho_0$ , where  $\rho_0$  is the electron density of amorphous silica.  $I_{\text{methyl}}(s)$  was approximated by a modified Percus–Yevick (PY) hard-sphere potential approach,<sup>13</sup> where polydispersity of sphere size was taken into account.<sup>9a</sup> The theoretical expression for the SAXS of this system is given by

$$I_{\text{methyl}}(s) = \frac{1}{\langle V_{\text{methyl}} \rangle_N} \{ \langle |F(s)|^2 \rangle + \langle F(s) \rangle^2 [S(s) - 1] \} \quad (2)$$

where  $F(s)$  represents the form factor of spheres with an average radius  $R$  and a variance  $\sigma$ ; while  $S(s)$  represents the structure factor according to the PY approach with the parameters  $R_{PY}$  and the volume fraction  $\phi$ .  $\langle V_{\text{methyl}} \rangle_N$  is the number average of the volume of CH<sub>3</sub> units. Assuming that the micropore content is sufficiently small to be modeled as a dilute system, their SAXS contribution is given by

$$I_{\text{micro}}(s) \approx \frac{\langle V_{\text{micro}}^2 \rangle_N}{\langle V_{\text{micro}} \rangle_N} \left( 1 - \frac{4}{3} \pi^2 R_g^2 s^2 + \dots \right) \quad (3)$$

where  $R_g$  is the radius of gyration of the micropores.

## 4. Results and Discussion

**4.1. TEM Study of the Mesostructure.** Figure 1 shows representative TEM micrographs of the calcined templated silica films prepared with MTES as silica precursor. As seen in the figure, the mesopores have nearly spherical shape with a certain ellipsoidal distortion, probably due to the stresses developed during the evaporation and condensation stages of the EISA process. These pores are uniform in size with average diameter of 5–7

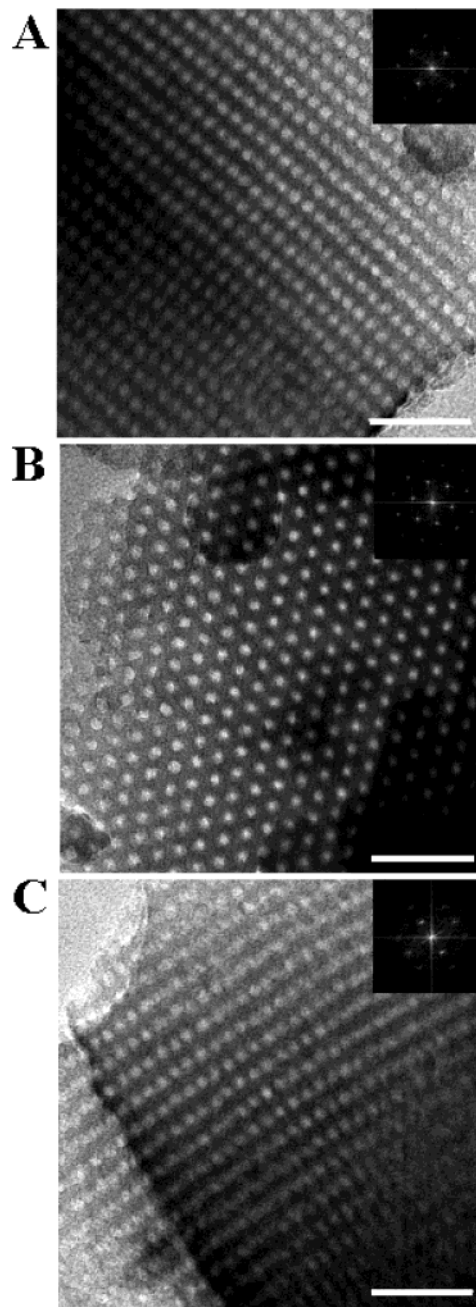


**Figure 1.** TEM images of calcined, PS-*b*-PEO-templated, MTES-derived mesostructured silica films. The copolymer: precursor weight ratio is 1:7 for panels A and B and 1:10 for panel C. The scale bar is 50 nm. The inset in each image is the Fourier transform derived from the entire area of each image.

nm and are arranged in highly ordered 3D hexagonal or tetragonal patterns with wall thickness of similar size. The mesopore arrangement is consistent with a bcc structure in all cases, and the orientation of each image can be indexed consistent with [011], [111], and [011] zone axes of the bcc structure, respectively. Very similar mesostructures were also obtained from a 40:60 MTES/TEOS mixture or pure TEOS as silica precursor (data not shown). A more detailed TEM study of these particular mesostructures, including film cross-sections, is under way and will be published elsewhere.<sup>14</sup>

**4.2. N<sub>2</sub> Sorption.** Figure 2 presents N<sub>2</sub> sorption isotherms at 77 K obtained with the SAW technique, for a PS-*b*-PEO-templated silica film with isolated spherical mesopores (curve I). The measurements essentially showed

(12) (a) Klotz, M.; Ayrál, A.; Guizard, C.; Cot, L. *Separ. Purif. Technol.* **2001**, *25*, 71. (b) Klotz, M.; Albouy, P. A.; Ayrál, A.; Menager, C.; Grosso, D.; Van der Lee, A.; Cabuil, V.; Babonneau, F.; Guizard, C. *Chem. Mater.* **2000**, *12*, 1721–1728.

(13) Percus, K. J.; Yevick, G. J. *Phys. Rev.* **1958**, *110*, 1.

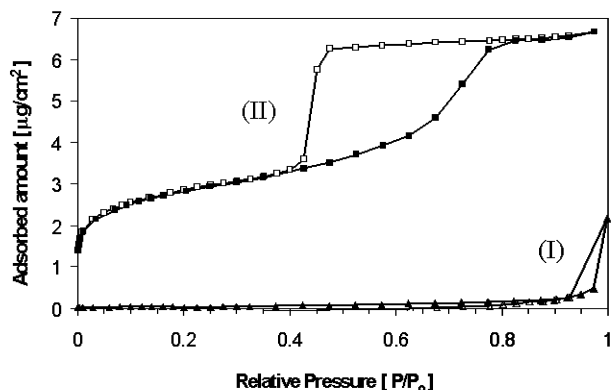


**Figure 2.** SAW  $N_2$  adsorption and desorption isotherms at 77 K for (I) the calcined MTES-derived templated silica film with ordered spherical mesopores shown in Figure 1A,B and (II) a calcined TEOS-derived templated silica film with hexagonally ordered cylindrical mesopores.<sup>6a</sup>

no  $N_2$  adsorption at relative pressures  $P/P_0 < 0.8$ , while a small hysteresis loop was observed at  $P/P_0 > 0.8$ , which is indicative of a mesoporous material with hindered nitrogen sorption. Since SAW measurements can be severely affected by the presence of cracks and other defects in the films, the experiments were repeated several times with good-quality films, resulting in similar sorption behavior in all cases.

To verify that the low  $N_2$  uptake of the film shown in curve I is not a result of the presence of defects in the film, a reference experiment was carried out with a PS-*b*-PEO-templated film prepared in the same way but having a mesostructure consisting of cylindrical mesopores organized in a hexagonal array, as a result of different surfactant concentration.<sup>6a</sup> In this case, a classical type IV  $N_2$  adsorption and desorption isotherm was observed (see curve II in Figure 2), which is indicative of a mesoporous material with high pore connectivity and accessibility. For this film, capillary condensation was observed at  $P/P_0 > 0.6$ , indicating the presence of mesopores larger than 5 nm.<sup>15</sup> The quantity of  $N_2$  absorbed at  $P/P_0 = 1.0$  by this film was about 6 times higher than that of the calcined film with isolated spherical mesopores (curve I).

These results illustrate that the accessibility of the spherical and cylindrical mesopores of the two films are significantly different for  $N_2$  at 77 K, suggesting a low interconnectivity of the mesopores of the films shown in Figure 1. These findings are also consistent with a previous study of nontemplated calcined silica thin films, where essentially no  $N_2$  adsorption at 77 K was detected by the SAW technique, indicating that the inorganic silica matrix is almost inaccessible by  $N_2$  at this temperature.<sup>7c</sup>

**4.3. Gas Permeation.** Figure 3A shows the gas permeation data as a function of kinetic diameter for the 50 Å  $\gamma$ - $Al_2O_3$  support and (1) a homemade  $C_6$ -surfactant templated microporous silica membrane<sup>7c</sup> with pores of size  $\sim 10$ – $15$  Å, (2) a homemade PS-*b*-PEO templated, MTES-derived silica membrane, (3) a nontemplated, MTES-derived microporous silica membrane,<sup>7b</sup> and (4) a nontemplated, TEOS-derived microporous silica membrane.<sup>7a</sup> The TEOS-derived microporous silica membrane (curve 4) exhibits a sharp decrease in permeance with increasing kinetic diameter and possesses pores of  $\sim 3.5$  Å, as judged by high permeance for He (2.6 Å),  $CO_2$  (3.3

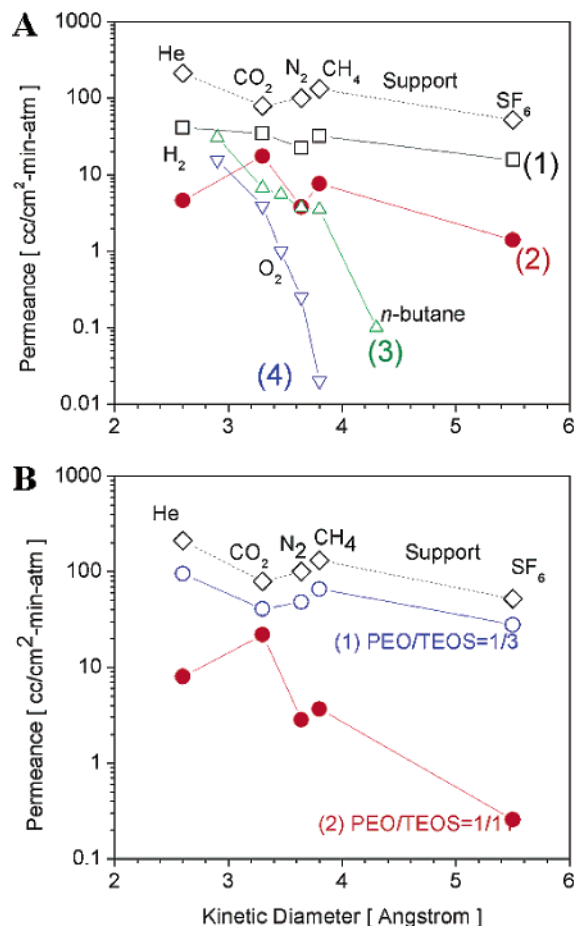


**Figure 3.** Single-gas permeance at 25 °C as a function of kinetic diameter of different silica-based membranes on 50 Å  $\gamma$ - $Al_2O_3$  support. (A) (1) Homemade  $C_6$  surfactant-templated microporous silica membrane<sup>7c</sup> with pores of 10–15 Å; (2) homemade PS-*b*-PEO-templated, MTES-derived silica membrane; (3) nontemplated, MTES-derived silica membrane<sup>7b</sup> with 4.0 Å pores; (4) nontemplated, TEOS-derived silica membrane<sup>7a</sup> with 3.5 Å pores. (B) Homemade, TEOS-derived PEO homopolymer-templated silica membranes prepared with PEO:TEOS weight ratios of 1:3 (1) and 1:11 (2). The permeance of the 50 Å  $\gamma$ - $Al_2O_3$  support is also shown in both figures.

Å), and  $O_2$  (3.46 Å) but lower permeance for  $N_2$  (3.64 Å) or even  $CH_4$  (3.8 Å). The MTES-derived microporous silica membrane (curve 3) possesses pores of  $\sim 4.0$  Å diameter, since it shows high permeance for He,  $CO_2$ ,  $O_2$ ,  $N_2$ , and  $CH_4$  but very low permeance for *n*-butane (4.3 Å). The microporous  $C_6$ -templated silica membrane (curve 1) shows permeance nearly independent of the kinetic diameter of the probe gases, which is consistent with a pore size being much larger than the kinetic diameter of the larger probe gas employed here,  $SF_6$  (5.5 Å).

The PS-*b*-PEO-templated MTES-derived silica membrane (curve 2) shows intermediate behavior compared to that of the microporous  $C_6$ -templated silica membrane (curve 1) and the nontemplated MTES- and TEOS-derived microporous silica membranes (curves 3 and 4). For example, the  $CO_2/SF_6$  pure gas permeation ratio of this membrane is as high as 14, whereas the respective ratio of the  $C_6$ -templated silica membrane is less than 2. Therefore, the 5–7 nm mesopores of the PS-*b*-PEO-templated silica membrane cannot form a continuous network throughout the membrane, because this would give rise to a  $CO_2/SF_6$  ratio not higher than 1.82, the theoretical value for Knudsen diffusion through mesopores

(14) (a) Yu, K.; Wu, X.; Brinker, C. J.; Ripmeester, J. *Langmuir* **2003**, *19*, 7282. (b) Wu, X.; Yu, K.; Brinker, C. J.; Ripmeester, J. *Langmuir* **2003**, *19*, 7289.

(15) Sing, K. S. W.; Everett, D. H.; Haul, A. W.; Moscou, L.; Pierotti, R. A.; Rouquerol, J.; Siemieniowska, T. *Pure Appl. Chem.* **1985**, *57*, 603.

of size  $>4$  nm.<sup>16</sup> On the other hand, the relatively high permeance of this membrane for SF<sub>6</sub> may suggest that this membrane consists of large micropores of size 6–10 Å or even microcracks, formed during the calcination step to remove the diblock copolymer from the membrane mesopores.

To obtain a better insight into the pore structure of the PS-*b*-PEO-templated silica membranes, we prepared silica membranes with TEOS as the silica source and PEO homopolymer (MW = 500) as the pore template. Figure 3B shows the gas permeation properties of these membranes for two different PEO/TEOS weight ratios. In the case of a high PEO/TEOS ratio (=1/3; curve 1), the membrane shows gas transport behavior consistent with permeation through large micropores or even mesopores, as evidenced by the weak dependence of permeance on probe gas kinetic diameter. On the other hand, the membrane made with low PEO/TEOS ratio (=1/11; curve 2) shows gas transport behavior consistent with permeation through micropores of size 6–7 Å, as evidenced by a much stronger dependence of permeance on probe gas kinetic diameter. For example, the CO<sub>2</sub>/SF<sub>6</sub> ratio for this membrane was as high as 100, whereas the SF<sub>6</sub> permeance itself was 2 orders of magnitude lower compared to the membrane with high PEO/TEOS weight ratio (curve 1).

The above results suggest that when a high amount of PEO is dispersed in a silica matrix, large micropores or even mesopores are formed, probably due to the PEO chains coiling and giving origin to pores of size related to the radius of gyration of the polymer chains. On the other hand, when a lower amount of PEO is used, the PEO chains may be more extended and hence micropores are formed related to the cross-sectional diameter of the PEO backbone, consistent with a previous report.<sup>9c</sup> In the case of PS-*b*-PEO-templated silica membranes, it is possible that a small portion of the PEO chains are frozen outside the spherical mesopores before complete retraction, giving rise to some connectivity of the large spherical mesopores through these smaller micropores.

Indeed, the shape of curve 2 in Figure 3A corresponding to the PS-*b*-PEO-templated silica membrane is very similar to curve 2 in Figure 3B, corresponding to the PEO-templated silica membrane, although the former shows SF<sub>6</sub> permeance about 1 order of magnitude larger than the latter. This higher SF<sub>6</sub> permeance of the PS-*b*-PEO-templated silica membrane could in part be attributed to the presence of the large spherical mesopores in the silica matrix (see Figure 1), giving rise to larger porosity and hence faster transport through this membrane. In addition, both membranes exhibit faster permeance for CO<sub>2</sub> compared to the lighter and smaller He, which indicates enhanced surface diffusion of the strongly adsorbing CO<sub>2</sub> through micropores of size  $<1$  nm.<sup>17</sup> Note that all the rest membranes shown in Figure 3 as well as the 50 Å  $\gamma$ -Al<sub>2</sub>O<sub>3</sub> support membrane show faster permeance for He, consistent with the presence of micropores  $<0.4$  nm (curves 3 and 4 in Figure 3A) or pores larger than 1 nm (curves 1 in Figure 3).

Further evidence for the above hypothesis can be inferred from the results of gas permeation in the presence of a condensable vapor (here ethanol) presented in Figure 4. As shown in the figure, curves 1 and 2 correspond to silica membranes templated by C<sub>6</sub> surfactant and PS-*b*-PEO diblock, respectively, while curve 3 corresponds to

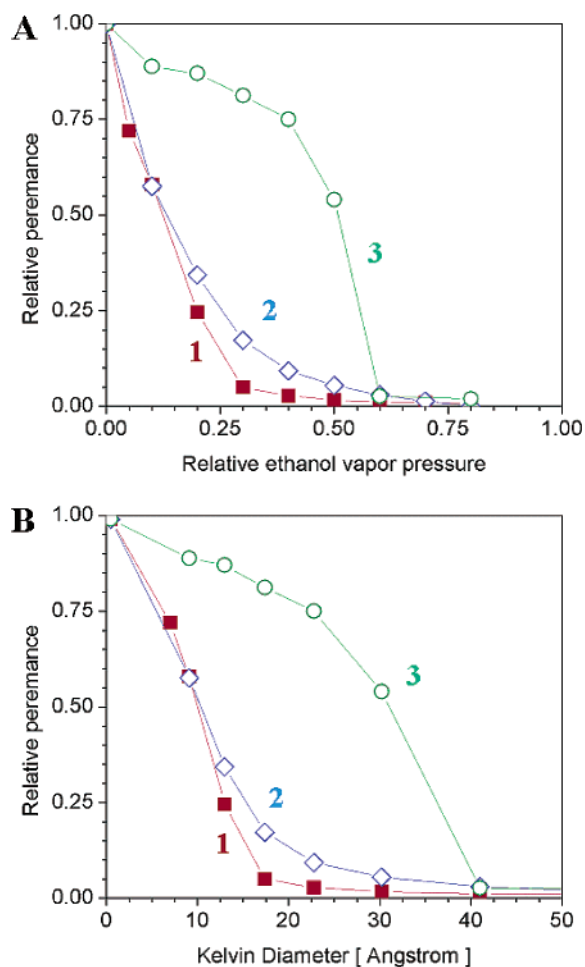


**Figure 4.** N<sub>2</sub> permeation experiments in the presence of condensable ethanol vapor as a function of (A) relative ethanol vapor pressure ( $P/P_{sat}$ ) or (B) corresponding Kelvin diameter. The membranes were (1) a homemade C<sub>6</sub> surfactant-templated microporous silica membrane<sup>7c</sup> with pores of 10–15 Å, (2) a homemade PS-*b*-PEO-templated, MTES-derived silica membrane, and (3) a commercial 50 Å  $\gamma$ -Al<sub>2</sub>O<sub>3</sub> membrane.

the commercial mesoporous (50 Å)  $\gamma$ -Al<sub>2</sub>O<sub>3</sub> support membrane. For the  $\gamma$ -Al<sub>2</sub>O<sub>3</sub> membrane, we observe that the permeance initially drops gradually for ethanol  $P/P_{sat} < 0.4$ , followed by a more rapid permeance loss and finally complete pore blockage at  $P/P_{sat} = 0.6$ . On the other hand, the templated silica membranes display a very sharp drop in permeance even at  $P/P_{sat} \rightarrow 0$ , followed by complete pore blocking at  $P/P_{sat} = 0.6–0.7$ . These results suggest that (i) the accessible pores in the PS-*b*-PEO-templated silica membrane are similar in size to the pores in the C<sub>6</sub>-templated membrane and (ii) the large spherical mesopores of this membrane cannot form a continuous network, otherwise a behavior similar to that of  $\gamma$ -Al<sub>2</sub>O<sub>3</sub> should be observed.

#### 4.4. GISAXS Study: Mesostructure Investigation.

Because the determination of the mesopore arrangement of the films shown in Figure 1 from TEM alone involves fundamental uncertainties, GISAXS experiments were carried out and a representative pattern is presented in Figure 5A, which is obtained from the calcined MTES-derived silica film shown in Figure 1C. Various experiments showed several characteristic diffraction spots, confirming a well-defined 3D mesostructure with a long-range order (Figure 5B). The solid dots correspond to the diffraction spots observed, while the dots with broken lines correspond to the diffraction spots hidden by the reflection of the primary beam. This 2D GISAXS pattern is consistent

(16) Nishiyama, N.; Park, D. H.; Koide, A.; Egashira, Y.; Ueyama, K. *J. Membr. Sci.* **2001**, *182*, 235.

(17) (a) Kusakabe, K.; Kuroda, T.; Morooka, S. *J. Membr. Sci.* **1998**, *148*, 13. (b) Flanders, C. L.; Tuan, V. A.; Noble, R. D.; Falconer, J. L. *J. Membr. Sci.* **2000**, *176*, 43. (c) Fuertes, A. B.; Menendez, I. *Separ. Purif. Technol.* **2002**, *28*, 29.

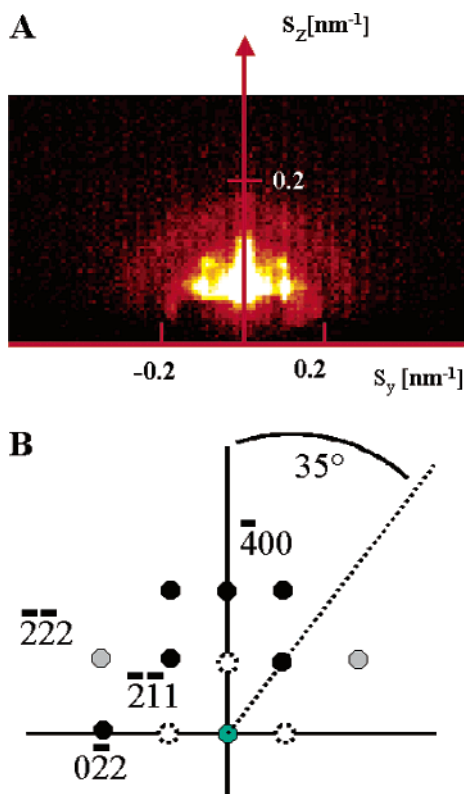


**Figure 5.** (A) Two-dimensional GISAXS pattern of the calcined, MTES-derived templated silica film seen in Figure 1C; (B) a sketch of all of the Bragg reflections observed from this sample. The pattern is consistent with a bcc structure under [011] orientation with a lattice parameter of 13 nm.

with a bcc structure in [011] orientation, thus supporting the TEM results shown in Figure 1. Similar GISAXS experiments verified the presence of long-range order in respective films deposited on porous  $\gamma\text{-Al}_2\text{O}_3$  supports used for the permeation studies in section 4.3.

#### 4.5. GISAXS Study: Microstructure Investigation.

Figure 6A presents radially averaged GISAXS data obtained from (1) a mesoporous silica powder described in ref 9, templated with PS-*b*-PEO and containing a substantial concentration of micropores; (2) a calcined templated silica film, see TEM in Figures 1A,B; (3) an uncalcined, nontemplated MTES-derived silica film; (4) a calcined, nontemplated TEOS-derived silica film; and (5) background scattering. Aside from the Bragg reflections at small  $s$  in curve 2, a broad maximum is observed at large  $s$  ( $\sim 0.95 \text{ nm}^{-1}$ ) in curves 2 and 3 that can be attributed to the average distance of the  $\text{CH}_3$ -ligands of the MTES precursor dispersed in the silica matrix, as proposed previously.<sup>6b</sup>

To confirm that the local maximum at  $s \sim 0.95 \text{ nm}^{-1}$  originates from the methyl ligands of the MTES precursor, we performed a GISAXS study of nontemplated MTES-derived silica films after calcination under different conditions. Curves 1, 2, and 3 in Figure 6B show the SAXS data of silica films calcined at 400 °C in Ar (standard calcination procedure), at 600 °C in Ar, and at 400 °C in air, respectively. It is seen that the local maximum at  $s \approx 0.95 \text{ nm}^{-1}$  almost disappears upon treatment at higher temperature or in the presence of oxygen (curves 2 and 3), indicating the decomposition of the MTES methyl ligands upon harsher calcination conditions.

In principle, the SAXS pattern at large  $s$  could be also influenced by microporosity in the inorganic matrix caused by the removal of the PEO block, referred to as PEO micropores. Curve 1 in Figure 6A shows the GISAXS data

obtained from a mesoporous silica powder described in ref 9, also templated with PS-*b*-PEO and containing a substantial concentration of micropores. At large  $s$ , a significant difference in the shape is observed between this curve and the GISAXS curve of the mesoporous film (curve 2), suggesting the absence of a large amount of PEO micropores in the latter. Similar GISAXS results were also obtained from mesoporous films prepared with pure TEOS as precursor.<sup>18</sup> In the following, a theoretical analysis is given with respect to the shape of the SAXS data at large  $s$ , determined by the methyl ligands and micropores, attempting to quantify an upper limit for the volume fraction of the latter in the PS-*b*-PEO-templated silica films.

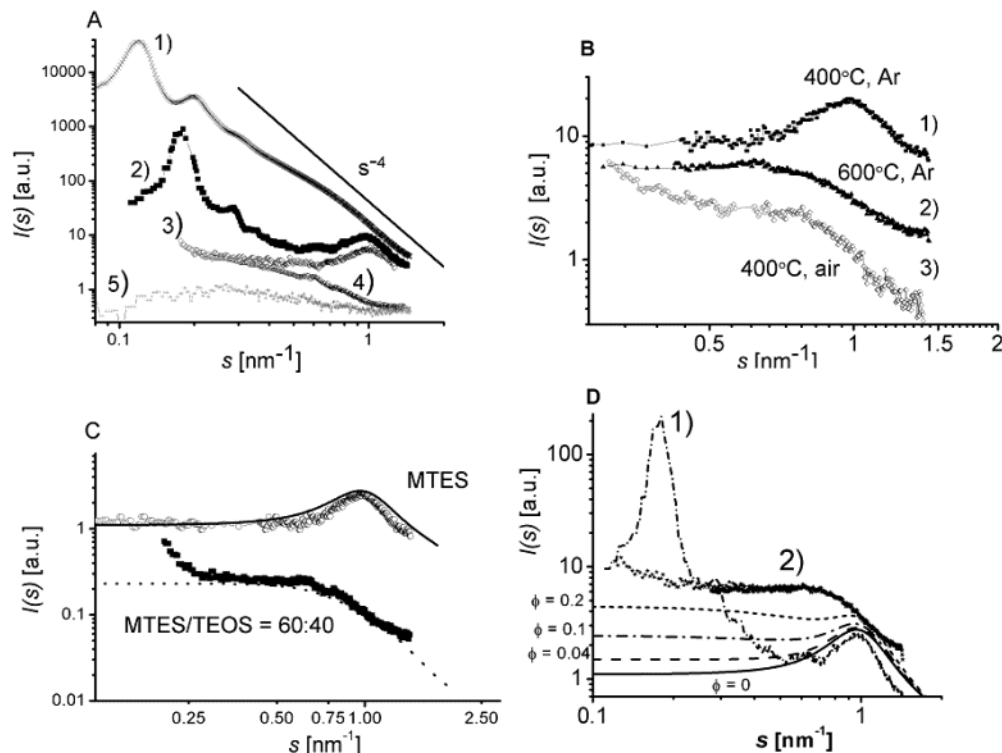
#### 4.6. Simulation of SAXS Data: (i) Methyl Ligands.

Figure 6C presents experimental GISAXS data for the nontemplated, MTES- and MTES/TEOS-derived silica films, together with the corresponding simulations based on the PY approach. For the MTES-derived films, we obtain  $R = 0.2 \text{ nm}$ ,  $\sigma_R = 0.03 \text{ nm}$ , PY radius  $R_{\text{PY}} = 0.43 \text{ nm}$ , and a volume fraction  $\phi_{\text{methyl}} = 0.15 \pm 0.05$ . For the MTES/TEOS-derived film, the corresponding parameters are  $R = 0.23 \text{ nm}$ ,  $\sigma_R = 0.05 \text{ nm}$ ,  $R_{\text{PY}} = 0.6 \text{ nm}$ , and  $\phi = 0.1 \pm 0.05$ . The fitted values for  $R$  are consistent with the size of the methyl ligand ( $\sim 0.4 \text{ nm}$ ) while the  $R_{\text{PY}}$  value for the MTES-derived film is consistent with the average distance between the centers of two  $\text{SiO}$  tetrahedra, being approximately 0.7–0.8 nm. A slightly higher value of  $R_{\text{PY}}$  (and a lower volume fraction  $\phi$ ) for the MTES/TEOS-derived film is also reasonable since the concentration of methyl ligands is lower in this film compared to the MTES-derived film. These results also confirm a random copolymerization of the MTES and TEOS precursors during film formation, as already proposed previously.<sup>19</sup> While the simulations provide good estimates for  $R$  and  $R_{\text{PY}}$ ,  $\phi$  and  $\sigma$  cannot be determined with similar accuracy. Nevertheless, these simulations indicate that the scattering contribution at large  $s$  in curves 2 and 3 of Figure 6A arise from the distribution of methyl ligands of the MTES precursor in the silica matrix, in agreement with the NMR results published previously.<sup>6b</sup>

**(ii) PEO Micropores.** Figure 6D presents (1) experimental GISAXS data of a PS-*b*-PEO-templated, MTES-derived mesoporous silica film and (2) experimental GISAXS data of a PEO-templated, TEOS-derived microporous silica powder with a PEO:TEOS ratio of 1:11 in the starting sol, together with several theoretical SAXS curves of a system of methyl ligands and PEO micropores of varying volume fraction of the latter, computed from eq 1. The electron density of  $\text{SiO}_2$  was calculated from the density of amorphous  $\text{SiO}_2$ , while  $\rho_{\text{methyl}}$  was estimated from the density of paraffin.  $I_{\text{methyl}}(s)$  was calculated from eq 2, assuming  $\langle v_{\text{methyl}} \rangle_N \approx 4/3\pi R^3$ , while the contribution from the PEO micropores,  $I_{\text{micro}}(s)$ , was computed from eq 3 assuming  $R_g = 0.5 \text{ nm}$ ,  $\langle v_{\text{micro}} \rangle_N \approx 0.65 \text{ nm}$  (obtained from Figure 6D, curve 2, assuming a spherical shape of the micropores), and  $\langle v_{\text{micro}}^2 \rangle_N \approx 1 \text{ nm}$  (estimate). The theoretical curves in Figure 6D indicate that a gradual increase of the volume fraction  $\phi$  of the PEO micropores leads to a progressively less pronounced peak at  $s \approx 1 \text{ nm}^{-1}$ , attributed to the methyl units. The scattering from micropores gives rise to a constant slope rather than a peak in this region, in agreement with the experimental curve 1 in Figure 6A. This simulation suggests that the volume fraction of the PEO micropores in the templated silica film should not exceed  $\phi = 0.04$ , otherwise the  $\text{CH}_3$  “peak” would be significantly less pronounced. In conclu-

(18) Smarsly, B.; Yu, K.; Brinker, C. J. *Stud. Surf. Sci. Catal.* **2003**, *146*, 295–298.

(19) Fyfe, C. A.; Aroca, P. P. *J. Phys. Chem. B.* **1997**, *101*, 9504.



**Figure 6.** (A) GISAXS patterns of a variety of silicas: (1) mesoporous silica reported in ref 9; (2) calcined, templated silica film shown in Figure 1A,B; (3) nontemplated, uncalcined MTES-derived silica film; and (4) a nontemplated, calcined TEOS-derived silica film; (5) background scattering. (B) GISAXS patterns of nontemplated, MTES-derived silica films calcined at (1) 400 °C in argon, (2) 600 °C in argon, and (3) 400 °C in air. (C) Experimental and simulated GISAXS patterns of (1) nontemplated, uncalcined MTES-derived silica film and (2) the corresponding MTES/TEOS-derived silica film. (D) Experimental GISAXS patterns of (1) PS-*b*-PEO templated, MTES-derived silica film and (2) PEO-templated, TEOS-derived silica powder with a PEO:TEOS weight ratio of 1:11. The solid, dashed, dashed-dotted, and dotted curves are PY simulations for different volume ratios  $\phi$  of PEO-micropores.

sion, also the GISAXS analysis supports the model of an array of isolated, cubic-ordered spherical mesopores of size 5–7 nm with the walls containing only a small number of PEO micropores of size up to 1 nm.

## 5. Conclusions

The meso- and microstructure of templated silica films prepared through evaporation-induced self-assembly (EISA), with MTES and/or TEOS as silica precursors and PS-*b*-PEO as structure-directing agent, were characterized by TEM, N<sub>2</sub> sorption, gas permeation, permporosimetry, and GISAXS. First, gas permeation and permporosimetry measurements of calcined templated films deposited on porous supports have turned out to be invaluable techniques to characterize the connectivity and porosity of the silica matrix surrounding the mesopores. According to these experiments, the mesopores of supported membranes cannot form a continuous network but may be interconnected through a small number of solvent or PEO-induced micropores of size up to 1 nm. Because of their size and number, these micropores are not detectable by N<sub>2</sub> sorption at 77 K but can be detected by gas permeation measurements at 25 °C, as suggested by the similarities in gas transport behavior of the PS-*b*-PEO-templated membranes with the PEO-templated membranes prepared at low PEO/TEOS weight ratio (see curves 2 in Figure 3). These micropores can also form a pathway for diffusion of the diblock decomposition products during calcination of thin films to remove the template from the nonconnected spherical mesopores.

Second, experimental and simulation GISAXS investigations confirm that only a small number of PEO micropores, with a content less than 4% by volume, are distributed in the silica matrix after calcination. Taking

into account the polymer content and the PEO fraction in the starting solution, it is estimated that ~20% of the PEO chains result in micropores, which is significantly less than in the case of the silica powder reported previously. As pointed out recently,<sup>6b</sup> this can be attributed to a retraction of the PEO chains from the silica matrix under the present self-assembly conditions.

In conclusion, our study also demonstrates for the first time how the combination of appropriate analytical techniques helps to quantitatively characterize mesoporous films in a comprehensive manner and provides guidance and methodology for the study of formation mechanisms and pore structures of other related mesoporous films prepared by similar self-assembly processes. Future work is also planned to further characterize the porosity of these films as well as films templated by other block copolymers, e.g., poly(isoprene)-*block*-poly(ethylene oxide).

**Acknowledgment.** This work was supported by Sandia National Laboratories, a Lockheed Martin Company, under DOE Contract DE-AC04-94AL85000; the Air Force Office of Scientific Research, Award F49620-01-1-0168; the DOE Office of Basic Energy Sciences; the DOD MURI Program, Contract 318651; Sandia's Laboratory Directed Research and Development Program; and the ARL Collaborative Technology Alliance in Power and Energy, Cooperative Agreement DAAD19-01-2-0010. We are indebted to Dr. Jun Liu and Dr. Ralf Koehn for useful discussions and to Dr. Alain Gibaud for assistance in the synchrotron experiments.